Lab on a Chip

ELECTRONIC SUPPLEMENTARY INFORMATION

Polymer-based microfluidic chip for rapid and efficient immunomagnetic capture and release of *Listeria monocytogenes*

Received 00th January 20xx,
Accepted 00th January 20xx

DOI: 10.1039/x0xx00000x

www.rsc.org/

L. Malic[a], X. Zhang[a], D. Brassard[a], L. Clime[a], J. Daoud[a], C. Luebbert[b], V. Barrere[b], A. Boutin[a], S. Bidawid[b], J. Farber[b], N. Corneau[b], and T. Veres[a,c,†]

1. M-chip Fabrication

M-chip device was fabricated by hot-embossing using a procedure similar to the one previously developed by our group.[35, 36] Briefly, SU-8 molds for the top and bottom substrates were fabricated using standard photolithography. The molds were subsequently treated with silane and replicated in PDMS using soft lithography.

For the top substrate structuring, casting protocol was used over the resulting PDMS structure to fabricate an epoxy mold for thermal polymer (TPE) replication by hot embossing. The epoxy mold was obtained by mixing at 65 °C the two epoxy material components; the resin FR–1080 Conapoxy® and the Conacure® hardener at a ratio of 100/83 by weight (Cytec Corp, Woodland Park, NJ). The composition was poured onto the PDMS substrate and cured for 12 h at 80 °C. After curing, the PDMS was peeled-off, and a final annealing step of 2 h at 120 °C was performed. The epoxy mold was subsequently used to emboss a Mediprene OF 400M SEBS (Styrene-Ethylene/Butylene-Styrene) TPE (Elasto AB Corp., Åmal, Sweden) substrate for 20 min at 140 °C and an applied pressure of 10 kN (EVG520, EV Group). The final shaping of all TPE components was accomplished using a dedicated cutter/puncher tool for the precise definition of the substrate shape and inlet/outlet through-hole structures.

For the bottom substrate structuring, a working stamp was obtained by UV curing for 5 min the photocurable polymer (Solvay MD700 with 1% Darocur 1173 photoinitiator) sandwiched between the silanized PDMS replica and a glass plate. Subsequently, the working stamp was employed to pattern a hard Zeonor™ substrate by hot-embossing at an applied pressure of 20 kN for 5 min at 160 °C to form the capture chamber containing a regular array of high aspect-ratio micropillars.

Post-embossing, the surface modification of the pillar region for subsequent nickel deposition was performed using oxygen plasma treatment for 10 minutes (Harrick Plasma, USA). For this purpose, the bottom substrate was masked in order to expose only the chamber area. The nickel deposition was subsequently achieved via an electroless process by using nickel sulfate electrolyte. The modified substrate was first activated with tin chloride and palladium chloride solutions in order to grow a monolayer of Pd nanoparticle seeds. The activated substrate was rinsed thoroughly by distilled water, and immediately immersed into the electrolyte maintained at 60-75 °C and pH 9-9 for the deposition of nickel. The thickness of nickel coating was precisely controlled by the plating time in order to deposit 2 µm thick film (Figure 1d and Figure SI1).
Following nickel deposition, the film was passivated using hydroxy-terminated tri(ethylene glycol) undecane thiol (HS-PEG-OH, Nanoscience, USA). Surface modification was carried out using in-situ chemical reduction with thiol adsorption from an aqueous acidic solution.[37] Briefly, the substrate was placed in an electrochemical cell containing a solution of 0.05 M Na_2SO_4 at pH 3 and held at -0.6 V vs. Ag/AgCl. HS-PEG-OH diluted to a concentration of 10 mM was added to the Na_2SO_4 solution to obtain a final concentration of 0.1 mM. Surface functionalization was carried out for 30 minutes to ensure uniform and stable monolayer formation. After surface modification, the substrate was washed with ethanol and dried under a stream of nitrogen. The resultant devices were assembled and stored at 4 °C. Figure SI4a shows the current response prior to and during PEG-OH self-assembly on a Ni plated M-chip. Upon the addition of the thiol-PEG-OH in ethanol solution to a 0.05 M Na_2SO_4 solution, the current magnitude decreased, which is attributed to surface adsorption. Following 25 minutes of thiol-PEG-OH addition, the curve reached saturation indicating full monolayer formation.

[a] *Life Sciences Division, National Research Council of Canada, 75 de Mortagne Boulevard, Boucherville, QC, J4B 6Y4, CANADA.*
[b] *Bureau of Microbial Hazards, Health Canada, 251 Sir Frederick Banting Driveway, Ottawa, ON, K1A 0K9, CANADA.*
[c] *Biomedical Engineering & Bioengineering Departments, McGill University, 845 Rue Sherbrooke Ouest, Montreal, QC, H3A 0G4, CANADA.*
† Corresponding author: teodor.veres@cnrc-nrc.gc.ca.

2. Preparation of ground beef capture medium

Lean ground beef was purchased from a local retail store and then distributed into plastic zipper bags and stored at - 80°C for future use. Due to limited sample requirements, we prepared smaller samples while keeping the same dilution ratio of 1:10. Aseptically, a sample was thawed and 10g of ground beef sample was added to 90 mL of PBS buffer into a stomacher bag (Whirl-pak, USA). Bags were then stomached with stomacher 400 BA 7021 (Seward, USA) at 180 rpm for 2 min. The homogenate was centrifuged at 1000 rpm for 3 min to remove large debris. Filtration was subsequently performed through a 5 µm filter to remove large beef debris. Filtered sample was then employed as a capture medium.

3. Numerical modelling

Numerical modeling was performed by using the commercial software Comsol Multiphysics (www.comsol.com) version 3.4. The complete magnetic transport problem has been divided into four distinct numerical models: (1) the magnetic field generated by the ferromagnetic plate system (the external magnetic field); (2) the magnetic field from the array of cylindrical soft magnetic shells (the internal magnetic field); (3) the microfluidic flow past the array of cylindrical pillars and (4) the magnetic transport of superparamagnetic particles in a high gradient magnetic field region.

3.1 External magnetic field

The magnetic field from the magnetic plate system is simulated with the Comsol module *Electromagnetics – Magnetostatics* by solving the equation

$$\nabla \times \left(\frac{1}{\mu_0}\nabla \times A_z\right) = \nabla \times \vec{M} \qquad (1)$$

for the z component A_z of the potential vector on a square computational domain ABCD as shown in Fig. SI6. μ_0 is the absolute magnetic permeability of vacuum and $\vec{M}$ the magnetization vector. Two rectangular regions EFGH and E'F'G'H' are considered at the centre of this computational domain to take into account the permanent magnets. The magnetization of these regions is set to $M = M_s = 1{,}074\ kA/m$ in the out-of-plane (Ox) direction. Outside these regions air with relative magnetic permeability $\mu_r = 1$ (thus $M = 0$) is considered. The magnetic regions are $1\ cm \times 5\ cm$ in size and placed at a distance of $5.8\ cm$ from each other. The size of the overall computational domain is AB=AD=50 cm. $H_x = H_y = 0$ are imposed as boundary conditions on all four boundaries (AB, BC, CD and DA).

3.2 Internal magnetic field

The same Comsol module (*Electromagnetics – Magnetostatics*) is used to solve Equation (1) for the internal magnetic field generated by the magnetic pillars. An array of three pillars (Fig. SI7) of $8\ \mu m$ radius coated with $2\ \mu m$ of Ni is considered at the centre of a square computational domain (EFGH) with the size EF=FG=400 μm. The distance between two neighbor pillars is $50\ \mu m$. The magnetization inside the magnetic shells of these pillars is set to $M_s = 512{,}980\ A/m$ while water with relative magnetic permeability $\mu_r = 1$ is considered in the rest of the computational domain. $H_y = 100\ kA/m$ and $H_x = 0$ are imposed on all EF, FG, GH and HE boundaries.

3.3 Microfluidic flow

For the microfluidic flow past the array of micropillars a smaller computational domain ABCD has been considered (Fig. SI7). The Navier-Stokes equation

$$\rho\vec{u} \cdot \nabla\vec{u} = \nabla\left[-pI + \eta\left(\nabla\vec{u} + (\nabla\vec{u})^T\right)\right] \qquad (2)$$

along with the continuity equation

$$\nabla\vec{u} = 0 \qquad (3)$$

are solved by using the Comsol module *MEMS Module – Microfluidics – Incompressible Navier-Stokes – Steady state analysis*. $\vec{u}$ in the above equations is the unknown velocity field while I represents the three-dimensional identity tensor. A dynamic viscosity $\eta = 0.001\ Pa \cdot s$ and density $\rho = 1000\ Kg/m^3$ along with a thickness of $72\ \mu m$ are considered in the subdomain calculation. An inlet boundary condition $U_0 = 1\ mm/s$ (for example) is imposed as normal inflow velocity. $AM \cup ND \cup BC$ are considered as symmetry boundaries. CD is set to *Outlet – Pressure, no viscous stress* while $\hat{MPN}$ is a no-slip boundary condition.

3.4 Magnetic transport

The same computational domain ABCD (Fig. SI7) used for the microfluidic flow is used to solve the convection-diffusion equation

$$\frac{\partial c}{\partial t} + \nabla \cdot \left(-D\nabla c - \vec{u}_m c\right) + \vec{u} \cdot \nabla c = 0 \qquad (4)$$

where c is the number concentration of magnetic particles in solution, D is the diffusion constant associated with the particles, $\vec{u}$ is the fluid velocity field – the solution of Eq. (2) – and u_m is the particle magnetic velocity whose components are given by

$$u_{mx} = -\frac{\mu_0 L(\vec{H}) m_p}{6\pi\eta R_p}\left(h_x\frac{\partial H_x}{\partial x} + h_y\frac{\partial H_x}{\partial y}\right)$$
$$u_{my} = -\frac{\mu_0 L(\vec{H}) m_p}{6\pi\eta R_p}\left(h_x\frac{\partial H_y}{\partial x} + h_y\frac{\partial H_y}{\partial y}\right) \qquad (5)$$

m_p and R_p are respectively the magnetic moment and radius of an individual particle while h_x and h_y are normalized values for the magnetic field components H_x and H_y. $L(\vec{H})$ is the well-known Langevin function

$$L(\vec{H}) = \coth\left(k_L|\vec{H}|\right) - \frac{1}{k_L|\vec{H}|} \qquad (6)$$

The constant $k_L = 1.26 \times 10^{-5} m/A$ is found by fitting Eq. (6) against the experimental magnetization curve for the magnetic particles (SI Figure 2c).

Equation (4) is solved by using the Comsol module *PDE Modes – PDE, Coefficient form – Time dependent analysis* with a diffusion coefficient $D = k_B T/6\pi\eta R_p$ and a damping (mass) coeffient $d_a = 1$. All other parameters (absorption coefficient, source term, mass coefficient and conservative flux terms) are set to zero. Dirichlet boundary conditions are considered along AB and BC boundaries ($c = c_0$) while Neumann boundary conditions are set on the other remaining boundaries.

These last three models corresponding to the internal magnetic field, microfluidic flow and magnetic transport calculations are assembled into a unique multiphysics model by using the Comsol *Store Solution* feature. The three models are solved successively and the solutions from the first two models stored and used to solve the final magnetic transport problem. Both magnetostatic and microfluidic problems are solved by using a *Stationary Solver* while the convection-diffusion problem associated with the magnetic transport is considered as *Time Dependent.* Convergence to a stable concentration distribution is evaluated by considering the integral of the concentration field over the domain Ω (see Fig. SI7)

$$F(t) = \int_{\Omega} c(x,y,t)d\Omega \qquad (7)$$

as a probe plot parameter.

Supplementary Figures

SI Figure 1. Scanning electron microscopy images showing (a) pillar array in the capture chamber of M-chip replicated in plastic after Ni deposition and (b) Zoomed-in region of the chip showing the total deposited Ni thickness (c) Experimental magnetization curve for the HGMS device. In-plane magnetization curves for the pillar array is compared to same thickness flat Ni film. Intensity of applied magnetic field is indicated with the dashed line. Percentage of magnetic saturation achieved by an applied magnetic field of 1.25 kOe is indicated on the graph.

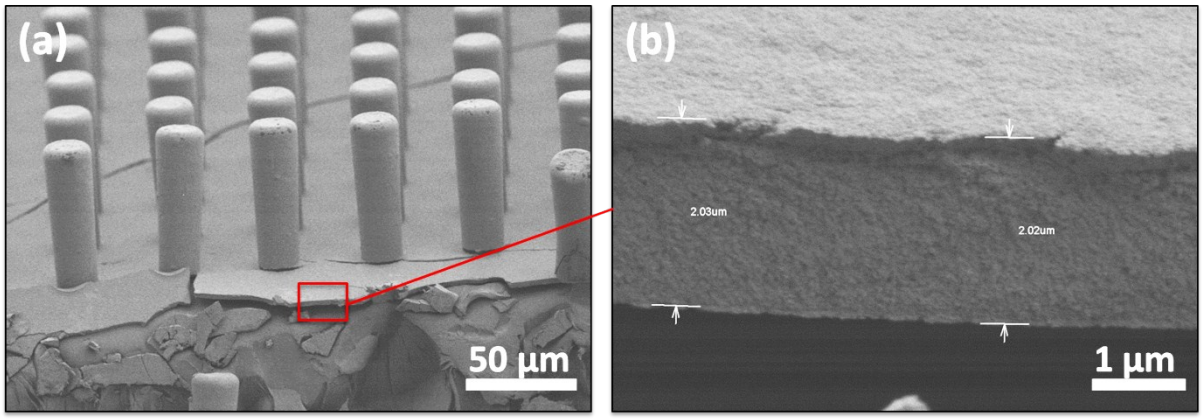

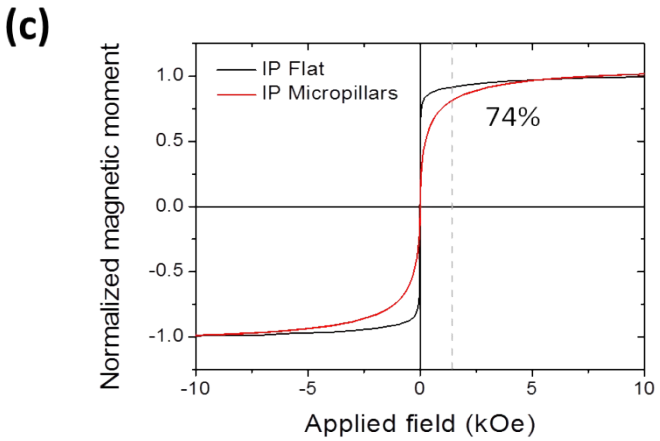

SI Figure 2. Numerical simulations of the magnetic field layout driving the M-chip magnetic capture: **(a)** Profiles of the magnetic field norm along Ox and Oy directions. Inset equations are used to indicate the values of the parasitic gradients generated by the magnetic system at $x = 8.5\ mm$ and $y = 15\ mm$ that correspond to the edges of the chip. **(b)** Magnetic field profile between two magnetized pillars from the point A located at the surface of the pillar to a point B on the symmetry plane indicated by the line (δ). Maximum value of the magnetic gradient at the surface of the pillar (point A) is indicated in the inset equation as well. **(c)** Schematic representations of a typical magnetic particle used in this study and experimental magnetization curve for 2.2 mg of solid state particle powder. Magnetic moment per unit mass (ρ_{mag}) obtained from this measurement is indicated in the inset equation.

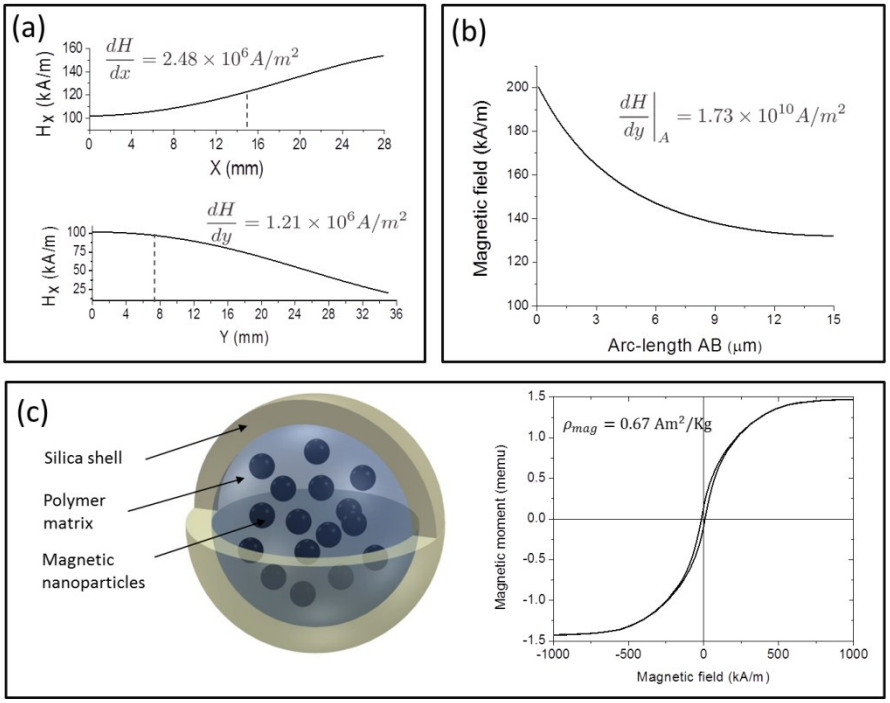

SI Figure 3. Time-lapse optical microscopy images showing clogging tests performed by flowing 6 ml of ground-beef filtrate (particulate size < 5 µm) through the M-chip at 100 µl/min for one hour.

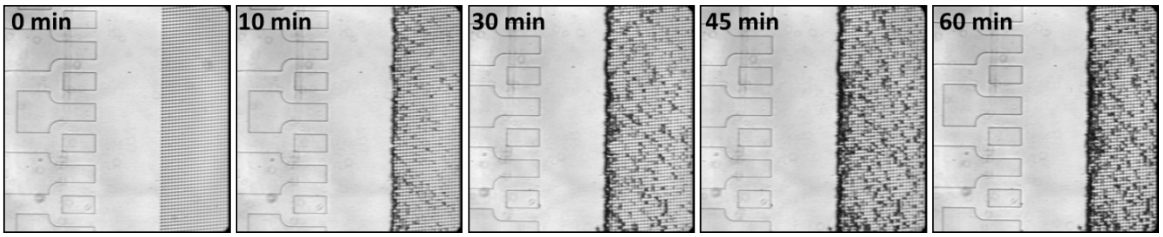

SI Figure 4. (a) Current signal plot for the M-chip Nickel surface passivation via in situ electrochemical reduction with PEG-OH-thiol adsorption from an aqueous acidic Na_2SO_4 solution at −0.6 V *vs.* Ag/AgCl. The current increases as a result of PEG-OH adsorption and becomes stable as the surface is saturated; **(b and c)** Fluorescence images showing the capture and release of stained dead *Listeria*-IMNP complex in buffer for the 10^5 cfu/mL concentration performed using **(b)** non-passivated M-chip surface and **(c)** passivated M-chip surface. The images were taken: *(i)* prior to the application of magnetic field; *(ii)* during the application of the magnetic field; and *(iii)* during the wash step, after the magnetic field has been removed; **(d)** A plot of normalized fluorescence intensity prior to capture, after capture and after release for non-functionalized and functionalized M-chip Ni surface.

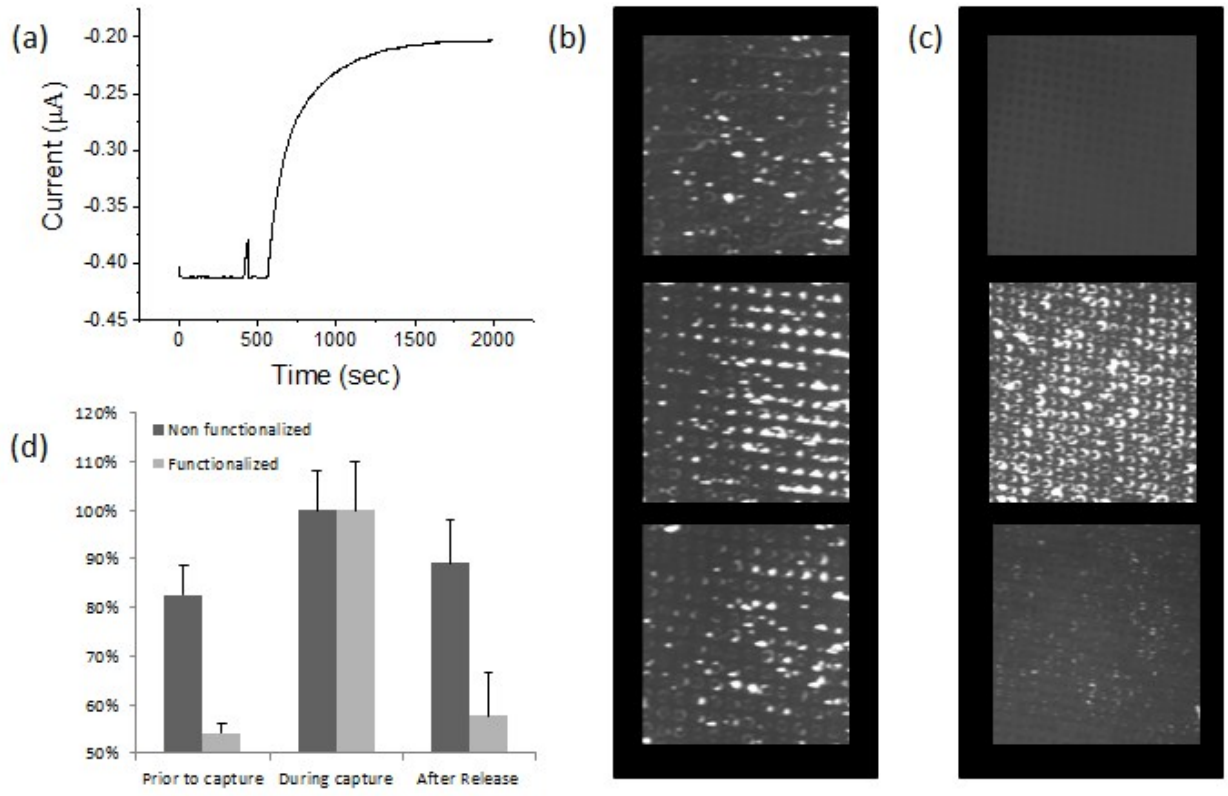

SI Figure 5. (a and b) SEM images of captured listeria-IMN complex agglomerate on the surface of the pillar.

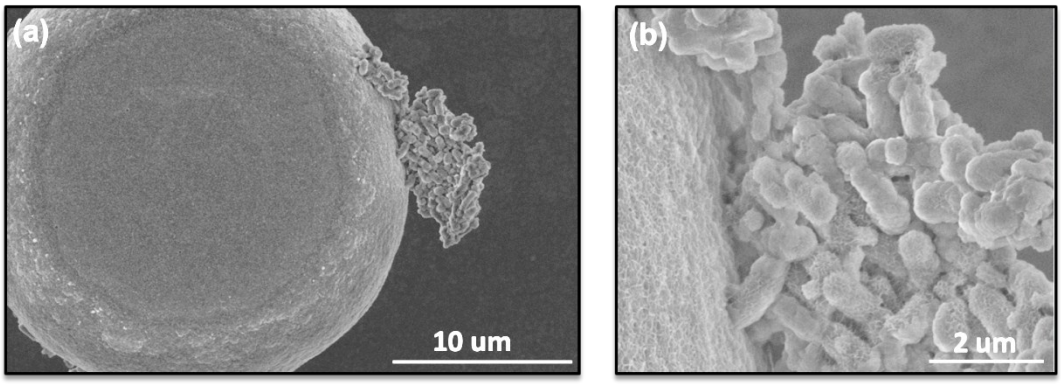

SI Figure 6. Computational domain used in the calculation of the external magnetic field generated by the two-plate magnetic system.

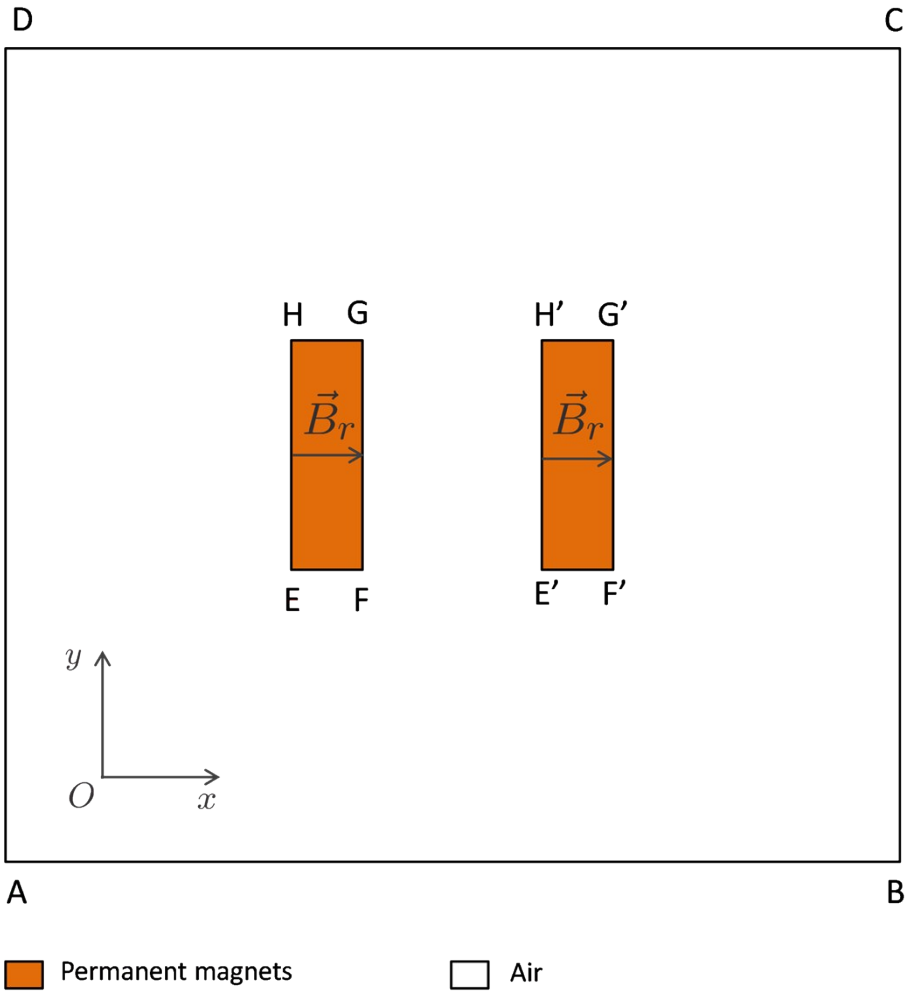

SI Figure 7. Computational domains used in the multiphysics numerical simulation related to the magnetic transport problem.